Mn Distribution and Spin Polarization in $Ga_{1-x}Mn_xAs$

Ruqian Wu

Department of Physics and Astronomy, University of California, Irvine, California 92697-4575, USA

(Received 13 November 2004; published 23 May 2005)

Using the density functional full-potential linearized augmented plane wave approach, the x-ray absorption and magnetic circular dichroism (XMCD) spectra of $Ga_{1-x}Mn_xAs$ are calculated. Significantly, XMCD of Mn is highly sensitive to the change in environment, and thus can be utilized to characterize impurity distribution. The nature of Mn-induced spin polarization on Ga and As sites, vital for the carrier mediated magnetic ordering, is discussed in light of computational and experimental results.

DOI: 10.1103/PhysRevLett.94.207201 PACS numbers: 75.25.+z, 71.20.Nr, 75.50.Pp, 78.70.Dm

Diluted magnetic semiconductors (DMS) form seamless hybrid structures on base semiconductors and hence promise high thermal stability and a high spin injection rate for spintronics applications [1,2]. Interestingly, the magnetic state in DMS can be manipulated by varying carrier density using light, co-doping, electric field and lattice strain [3–5]. The exploitation of DMS, however, is severely hindered by low Curie temperature, the lack of understanding of the mechanism of magnetic ordering, and difficulty in growth control. The origin of ferromagnetism in DMS remains an issue of active debate despite extensive theoretical and experimental explorations [6,7]. $Ga_{1-x}Mn_xAs$, a prototype DMS [8–10], is believed to have intrinsic magnetization with Mn impurities uniformly substituting Ga sites. However, no strong evidence is available to directly confirm these conjectures. Even Mn distribution, a prerequisite for studies of other electric and magnetic properties, remains unclear. Despite the fact that many density functional calculations have been done for $Ga_{1-x}Mn_xAs$ [11–15], an understanding of Ga and As magnetization away from magnetic impurities is still far from apparent.

Soft x-ray magnetic circular dichroism (XMCD), a powerful tool to explore magnetic and electronic properties with element selectivity, permits direct detection of Ga and As magnetization and is very important for studies of DMS as reported recently [16,17]. An unambiguous explanation for these results, nevertheless, usually relies on theoretical calculations using modern density functional approaches. Theoretical results reported in this Letter demonstrate that, for the first time, XMCD spectra can also be useful to identify Mn distribution in $Ga_{1-x}Mn_xAs$ since the spectroscopic features are highly sensitive to the change in atomic arrangements. The $Mn_{Ga} + Mn_I$ dimers are found to be the major defects in unannealed $Ga_{1-x}Mn_xAs$ samples. Furthermore, the dimer induced gap states are strongly localized around the interstitial Mn_I atoms, and hence they do not compensate the holes induced by the substitutional Mn_{Ga} monomers. This work lays a basis for the utilization of XMCD in studies of impurity distribution, along with electronic and magnetic properties, in $Ga_{1-x}Mn_xAs$ and related systems.

The all-electron full-potential linearized augmented plane wave (FLAPW) method was employed [18] in the present calculations. No shape approximation was assumed in charge, potential, and wave function expansions. The core states were treated fully relativistically while the spin-orbit interaction among valence states was invoked second variationally in the charge self-consistency loop [19]. The generalized gradient approximation in the formula of Perdew-Burke-Ernzerhof [20]) was adopted to describe the exchange-correlation interaction. Energy cutoffs of 225 and 12 Ry were chosen for the charge-potential and basis expansions in the interstitial region. In the muffin-tin region, spherical harmonics with a maximum angular momentum quantum number of $l_{max} = 8$ were used. We optimized the lattice constant and atomic positions through total energy minimization guided by the calculated atomic forces.

We first investigated uniform doping cases with a $Ga_{15}Mn_1As_{16}$ unit cell ($x = 0.0625$) shown in Fig. 1. The optimized lattice constant is 10.68 a.u., very close to the experimental data for this concentration, 10.7 a.u. The calculated x-ray absorption spectroscopy (XAS) and XMCD spectra of the L_3 edge are presented in Fig. 2 for Mn, As, and Ga atoms accompanied by the corresponding experimental data for unannealed $Ga_{1-x}Mn_xAs$ samples with $x = 0.07$. Uniform substitution of Mn on the Ga sites, denoted as Mn_{Ga} below, results in a double-peak profile in both XAS and XMCD spectra (thin solid lines), substantially different from the single peak profile of the experimental curves. Results with core-hole relaxation invoked in the self-consistent loop (thin dashed lines in Fig. 2(a)] indicate that the final state effects are not responsible for this discrepancy. Nonetheless, the total energy difference between the excited and ground states, 636.3 eV, is in an accurate agreement with the threshold position of experimental XAS/XMCD curves. The initial state calculations appear to be sufficient to determine the spectroscopic profiles of XMCD and XAS of $Ga_{1-x}Mn_xAs$ and likely other DMS. Nonetheless, one needs to shift the spectra obtained from initial state calculations by 15.5 eV for Mn, 23.2 eV for Ga, and 36.2 eV for As to the high-energy side to compensate the final state effects in $Ga_{1-x}Mn_xAs$.

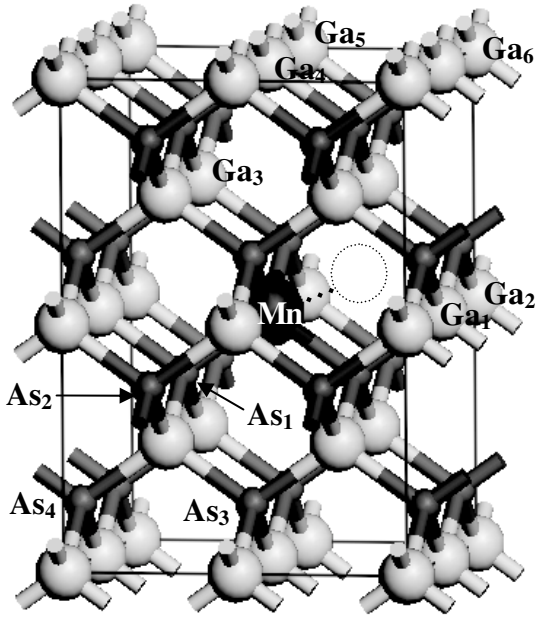

FIG. 1. Schematic unit cell used in the present calculations and notations of atoms for discussions in the text. Dashed circle indicates the position of Mn_I in Mn_{Ga} + Mn_I dimer.

In order to reveal the origin of discrepancy in spectroscopic profiles, we explored many different possibilities such as antisite defects, interstitial Mn, as well as various Mn dimers. Intriguingly, the spectroscopic features of Mn-XMCD are very sensitive to the change in environment around Mn, shown by the drastic differences in XAS and XMCD curves in Fig. 2(a). This promises a potential to use XMCD for unambiguous determination of impurity distribution in DMS through strong interplay between experiment and theory. For example, results for isolated interstitial Mn, thin dotted lines in Fig. 2(a), differ drastically from the experimental data. One can comfortably rule out the existence of this configuration in real samples. As-antisite defects, most likely to form on the Ga_1 and Ga_4 sites [21] from the point of view of total energy, are found to reduce the energy separation between two peaks in the XMCD curves (not shown here). Dimers of Mn_{Ga}-Mn_{As}, with two Mn atoms substituting adjacent Ga and As sites, provide a single peak XMCD profile by mixing with Mn_{Ga} results, but it is difficult to match the peak positions for XAS and XMCD simultaneously with the experimental curves. In contrast, results for Mn_{Ga}-Mn_I dimers, shown as dot-dashed lines in Fig. 2(a), closely resemble the experimental data. Here, the satellite Mn_I is placed at the center of the Ga tetrahedron, shown as the dashed circle in Fig. 1. The best fit to experimental Mn-XMCD curves can be achieved by mixing 50–50 of results calculated for Mn_{Ga} monomers and Mn_{Ga}-Mn_I dimers, displayed as the bold line in Fig. 2(a). Even the minutiae of experimental curves are satisfactorily reproduced. Furthermore, FLAPW calculations also satisfactorily reproduce the features of experimental XAS and XMCD spectra of As and Ga atoms

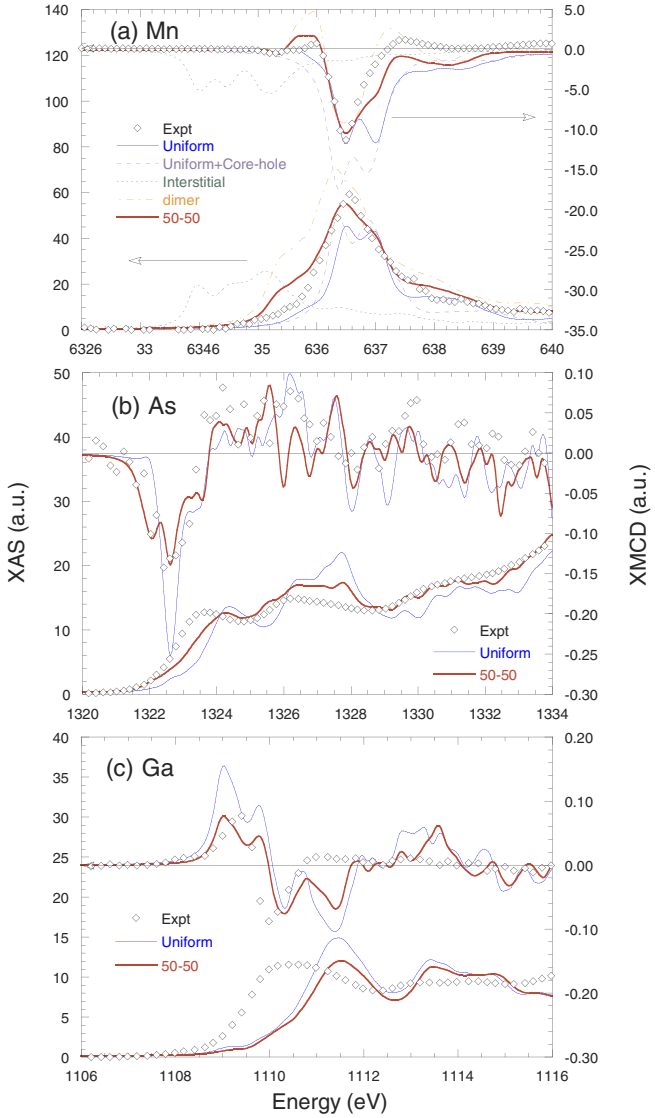

FIG. 2 (color online). The calculated XAS and XMCD spectra for Mn, As, and Ga for various doping cases as indicated by the legend, accompanied by the corresponding experimental data (symbols) which are rescaled in amplitude (with the same factor for XAS and XMCD). Meanwhile, theoretical spectra from initial state calculations are shifted by 15.5 eV for Mn, 23.2 eV for Ga, and 36.2 eV for As to consider the final state effects.

with 50–50 mixing, as displayed in Figs. 2(b) and 2(c) (bold lines versus symbols). Through present calculations, this is the only configuration that gives satisfactory spectroscopic results for all three elements. One can thus perceive that in the as-grown $Ga_{1-x}Mn_xAs$ samples the major defects are Mn_{Ga} + Mn_I dimers. This picture is also in good accordance with experimental results of low hole concentration and channeling Rutherford backscattering measurements [22], but the evidence here is much straighter.

From Table I, the magnetic moment in the unit cell is also sensitive to the change in local environment. As

TABLE I. The calculated magnetic moments, M (in μ_B/cell), for different configurations.

System	Mn_{Ga}	Mn_I	$Mn_{Ga} + As_{Ga}$	$Mn_{Ga} + Mn_I$	$Mn_{Ga} + Mn_{As}$
M (μ_B)	4.0	3.1	4.5–4.8	0.8	1.3

reported before, the magnetic moment of Mn is $4.0\mu_B$ for the uniform doping case (Mn^{+2}). The magnetic moments are noninteger in other cases, $3.1\mu_B$ in the interstitial site, and $(4.5–4.8)\mu_B$ when As-antisite defects are involved without considering disordered alignments [10]. Mn dimers are antiferromagnetic in GaAs, and their magnetic moments are small due to mutual cancellation. For example, one $Mn_{Ga} + Mn_I$ dimer contributes only $0.8\mu_B$, while one $Mn_{Ga} + Mn_{As}$ dimer gives $1.3\mu_B$. The presence of $Mn_{Ga} + Mn_I$ dimers is expected to drastically reduce the effective magnetic moment, as observed in most experiments [$(2.2–2.4)\mu_B$].

Results resolved into different atoms indicate that As_1 provides the leading contribution to the As XMCD spectrum. In contrast, the positive onset for Ga involves almost all Ga atoms. Even Ga_6 (15 a.u. away from Mn) gives a contribution comparable to Ga_1 (7.5 a.u. away from Mn), indicating the long-range nature of Mn-induced magnetization in the Ga sublattice. The l-project density of states (DOS) curves plotted in Figs. 3(a)–3(c) are for the uniform doping case with the $Ga_{15}Mn_1As_{16}$ unit cell. For Mn, the two pronounced minority spin peaks in the unoccupied region are responsible for the double-peak structure of the XAS/XMCD spectra in Fig. 2. These two states also have significant p components, and extend far into the As and the Ga regions. Subsequently, they result in the prominent $d(As_1)$ and $s(Ga_1)$ peaks around 1 eV in Figs. 3(b) and 3(c). These Mn-induced gap states, 100% spin polarized, produce the onsets of the XMCD spectra of As and Ga.

From Fig. 3(a), it is obvious that the carriers in the uniform $Ga_{1-x}Mn_xAs$ are p-like majority spin holes. In the As sublattice, the amplitude of DOS at E_f is large but decays rapidly away from Mn as indicated by the difference between the bold and thin lines for As_1 and As_4. In contrast, the value of DOS at E_f for Ga_6 is even slightly larger than that for Ga_1. These p-like states, perhaps the most important ones to mediate long-range magnetic ordering in $Ga_{1-x}Mn_xAs$, can be detected only through K-edge XMCD according to the selection rules. The amplitudes of K-edge XMCD in Fig. 4 for the $Ga_{15}Mn_1As_{16}$ unit cell appear to be extremely weak (0.2% of XAS for Ga and 1%–2% for As and Mn) but are still meaningful within 3 eV from the onset. Again, the K-edge XMCD signal of Ga_6 is stronger than that of Ga_1. Apparently, the p-like hole states carry spin polarization away from magnetic dopants through As in short range but more likely through Ga in long range.

Finally, Fig. 3(d) indicates that the carriers around $Mn_{Ga} + Mn_I$ dimers are electrons but they are confined around Mn_I. The presence of Mn_I shifts the d bands of Mn_{Ga} downward by 1 eV. No significant s- or p-like Mn state can be found around the Fermi level. Actually, the values of DOS at E_f are almost zero for remote As and Ga atoms such as As_4 and Ga_6. This suggests the strong localization feature of gap states induced by $Mn_{Ga} + Mn_I$ dimers, which should neither mediate exchange interaction

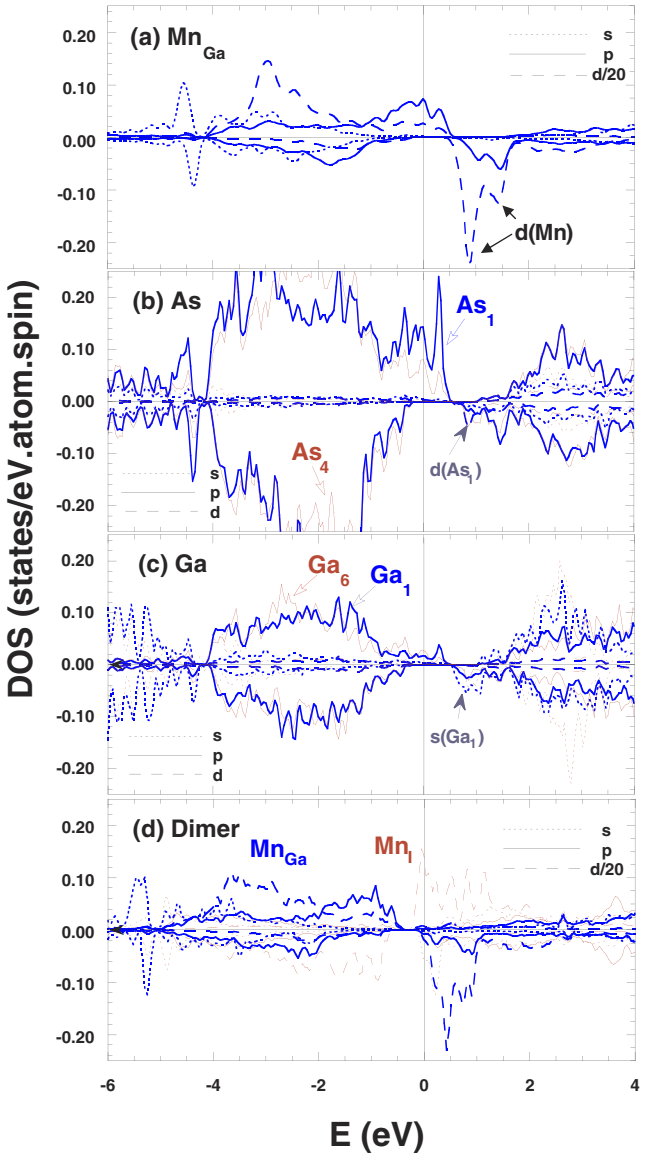

FIG. 3 (color online). The density of states for Mn, As, and Ga in uniform [in panels (a), (b), and (c)] and dimer [in panel (d)] doping cases. Positive and negative sides are for the spin-up and spin-down parts, respectively. The amplitude for Mn d states in panels (a) and (d) are rescaled by a factor of 1/20. Arrows point out either atoms that the DOS curves belong to or important states for XMCD.

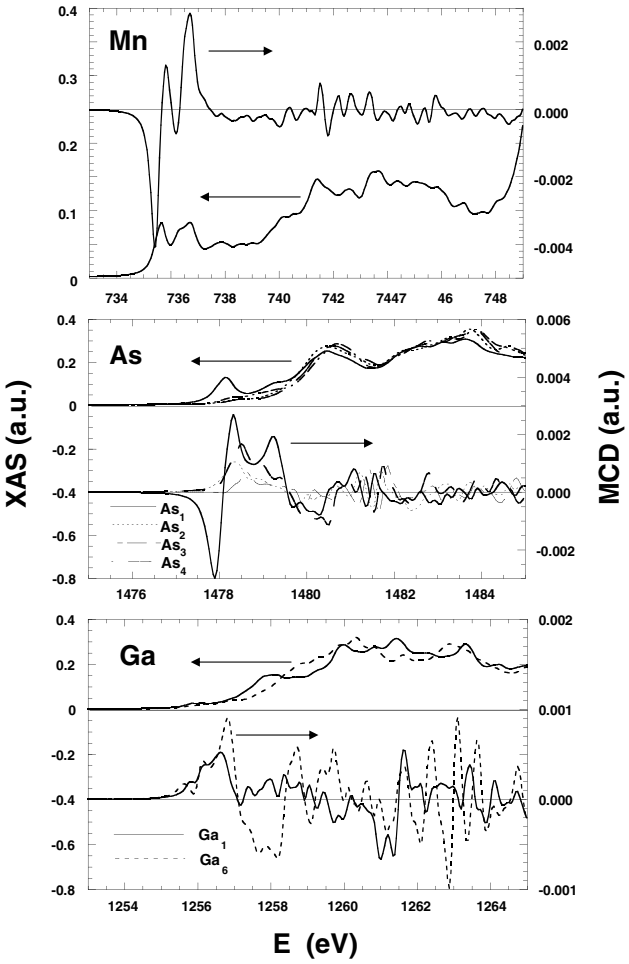

FIG. 4. The calculated initial state K-edge MCD spectra for Mn, As, and Ga atoms in the uniform doping case. No energy shift or amplitude rescaling was applied.

nor compensate the hole states induced by the Mn_{Ga} monomers. The effective carrier density in $Ga_{1-x}Mn_xAs$ is thus close to the concentration of Mn_{Ga} monomers alone, instead of the difference between concentrations of Mn_{Ga} monomers and $Mn_{Ga} + Mn_I$ dimers as perceived from a simple argument based on the double donor (Mn_I) versus single acceptor (Mn_{Ga}) picture.

In conclusion, we explored the magnetic properties of $Ga_{1-x}Mn_xAs$ ($x = 0.0625$) in different configurations. It was found that the spectroscopic profile of L-edge XAS and XMCD is highly sensitive to the change in Mn arrangement which, furthermore, is used to identify that Mn_{Ga}-Mn_I dimers are the major defects in unannealed samples. With close interplay between theory and experiment, XMCD can be exploited as a powerful tool to characterize impurity arrangements in DMS, currently still a difficult task for other techniques.

The author is indebted to Professor J. Shi at the University of Utah and Dr. D. Keavney at Argonne National Laboratory for providing experimental data and helpful discussions.

[1] D. D. Awschalom *et al.*, Phys. Today **52**, No. 6, 33 (1999); Nature (London) **397**, 139 (1999); **411**, 770 (2001).
[2] H. Ohno *et al.*, Science **281**, 951 (1998); Nature (London) **402**, 790 (1999); Science **291**, 840 (2001); IEEE Trans. Nanotechnol. **1**, 19 (2002).
[3] S. Koshihara *et al.*, Phys. Rev. Lett. **78**, 4617 (1997).
[4] A. Oiwa, Y. Mitsumori, R. Moriya, T. Slupinski, and H. Munekata, Phys. Rev. Lett. **88**, 137202 (2002).
[5] D. Chiba, M. Yamanouchi, F. Matsukura, and H. Ohno, Science **301**, 943 (2003).
[6] T. Dietl, H. Ohno, F. Matsukara, J. Clbert, and D. Ferrand, Science **287**, 1019 (2000).
[7] J. König, H. H. Lin, and A. H. MacDonald, Phys. Rev. Lett. **84**, 5628 (2000).
[8] H. Ohno, A. Shen, F. Matsukura, A. Oiwa, A. Endo, S. Katsumoto, and Y. Iye, Appl. Phys. Lett. **69**, 363 (1996); D. Chiba, K. Takamura, F. Matsukura, and H. Ohno, Appl. Phys. Lett. **82**, 3020 (2003).
[9] E. J. Singley, R. Kawakami, D. D. Awsholom, and D. N. Basov, Phys. Rev. Lett. **89**, 097203 (2002).
[10] L. Bergqvist *et al.*, Phys. Rev. B **67**, 205201 (2003).
[11] M. Jain, L. Kronik, J. R. Chelikowsky, and V. V. Godlevsky, Phys. Rev. B **64**, 245205 (2001).
[12] P. A. Korzhavyi *et al.*, Phys. Rev. Lett. **88**, 187202 (2002).
[13] Y. J. Zhao, W. T. Geng, K. T. Park, and A. J. Freeman, Phys. Rev. B **64**, 035207 (2001).
[14] S. Sanvito, P. Ordejon, and N. A. Hill, Phys. Rev. B **63**, 165206 (2001).
[15] M. van Schilfgaarde and O. N. Mryasov, Phys. Rev. B **63**, 233205 (2001).
[16] D. J. Keavney, D. Wu, J. W. Freeland, E. Johnston-Halperin, D. D. Awschalom, and J. Shi, Phys. Rev. Lett. **91**, 187203 (2003).
[17] K. W. Edmonds *et al.*, Appl. Phys. Lett. **84**, 4065 (2004).
[18] E. Wimmer, H. Krakauer, M. Weinert, and A. J. Freeman, Phys. Rev. B **24**, 864 (1981); M. Weinert, E. Wimmer, and A. J. Freeman, Phys. Rev. B **26**, 4571 (1982); M. Weinert, J. Math. Phys. (N.Y.) **22**, 2433 (1981).
[19] R. Q. Wu and A. J. Freeman, J. Magn. Magn. Mater. **200**, 498 (1999).
[20] J. P. Perdew, K. Burke, and M. Ernzerhof, Phys. Rev. Lett. **77**, 3865 (1996).
[21] The formation energy of the As-antisite defect is the lowest on the Ga_1 site. It is 0.36 eV higher on the Ga_4 site while it is 1.3–1.8 eV higher on the other Ga sites.
[22] K. M. Yu *et al.*, Phys. Rev. B **65**, 201303(R) (2002).